THE ASTROPHYSICAL JOURNAL, 466:473–486, 1996 July 20

THE SPATIAL DISTRIBUTION OF PARTICLES ACCELERATED BY CORONAL MASS EJECTION–DRIVEN SHOCKS

D. V. REAMES, L. M. BARBIER, AND C. K. NG[1,2]
NASA/Goddard Space Flight Center, Greenbelt, MD 20771
Received 1995 August 10; accepted 1995 October 24

ABSTRACT

We use multispacecraft observations to examine the spatial and temporal distributions of energetic particles accelerated by shock waves driven by coronal mass ejections from the Sun. The behavior of the intensity time profiles ahead of the shock can depend strongly on the longitude of the point where the observer's magnetic flux tube connects to the shock, relative to the nose of the shock where acceleration is strongest. Particle intensities can increase (decrease) with time as this point swings eastward through $\geq 50°$ toward (away from) the shock nose because of solar rotation. Well behind the shock, intensities are often constant with longitude and the intensities of these quasi-trapped particles at all energies decrease continuously with time over many days as their containment volume expands. Delayed proton events are produced when shocks expand into slow solar wind so they suddenly encounter an observer's field line far from the Sun. Sunward flows are seen when the shock passes over the observer or when it suddenly strikes his field line at radial distances out beyond him.

Subject headings: acceleration of particles — shock waves — Sun: corona — Sun: particle emission

1. INTRODUCTION

Recent years have brought a flood of new evidence suggesting that, in large solar energetic particle (SEP) events, particles from ~1 MeV to ~20 GeV are actually accelerated at a shock wave driven out by a coronal mass ejection (CME); they do not come from solar flares (see reviews by Reames 1992, 1993, 1994, 1995; Kaler 1992; Gosling 1993). While the importance of shock acceleration of ions actually was recognized (Wild, Smerd, & Weiss 1963) early in radio observations of solar events, the idea was apparently lost among two decades of diffusion models attempting to fit the intensity-time profiles of energetic protons. In these phenomenological multiparameter models, particles were presumed to come from a flare, diffuse across magnetic field lines in the corona, leak into interplanetary space, and then diffuse out to the observer. The models did not seek to understand the physical mechanisms of acceleration or of transport across magnetic field lines; the "flare myth" (Gosling 1993) was simply accepted. It was known, however, that the average abundances of elements in these large events seemed to reflect element abundances of the solar corona (Meyer 1985).

In 1970 Hsieh & Simpson (1970) first observed solar ^{3}He-rich events, energetic-particle events with 1000-fold enhancements in ^{3}He/^{4}He and 10-fold enhancements in Fe/O. The events had large electron intensities (Reames, von Rosenvinge, & Lin 1985) that provided accurate timing information and facilitated their association with type III radio bursts (Reames & Stone 1986) and impulsive X-ray flares (Reames et al. 1988). These events had impulsive particle profiles and were observed only from magnetically well-connected flares. Why did *these* particles not slowly diffuse across the corona or out into interplanetary space? The abundances seemed to distinguish two distinct acceleration mechanisms. If ^{3}He-rich particles came from flares, perhaps the particles in the large gradual SEP events had a different source.

In contrast, the large gradual SEP events showed a 96% association with CMEs (Kahler et al. 1984, 1987), though only the largest, fastest ~5% of CMEs, capable of driving coronal and interplanetary shock waves, had associated SEP events (Kahler 1992; Reames 1993). Most interesting are the erupting filament events (Kahler et al. 1986) that produce CMEs, shocks (type II radio bursts), gradual X-ray events, and characteristic gradual SEP intensity profiles (Reames 1993), but have no impulsive flare.

Ionization states of Fe are a particularly sensitive measure of the electron temperature of the source plasma at coronal and flare temperatures. Luhn et al. (1985) measured the ionization states of the elements from C through Fe in 12 SEP events. The mean charge of Fe, 14.9 ± 0.1, represents a temperature of ~2 MK that is not unlike the temperature of the ambient corona. In fact, the ionization states of all of the elements in these events were similar to those of ions in the solar wind. There was no evidence here for the hot plasma that would be expected in a flare or reconnection region. More recently, Tylka et al. (1995) have found a mean charge of 14.2 ± 1.4 for 200–600 MeV amu^{-1} Fe ions from three large SEP events in 1989 September and October. Thus, flare-heated material is not present at extremely high energies, either. In contrast, however, the Fe observed in ^{3}He-rich events has charge 20.5 ± 1.2, and elements up through Si are fully ionized (Luhn et al. 1987), indicating either a plasma temperature of ~20 MK or stripping by the intense electron beams (Miller & Viñas 1993) in these impulsive-flare events.

Thus the wide longitude spread and long time profiles, the low charge states, the strong association with CMEs, type II and IV radio bursts, and interplanetary shocks have led to the new paradigm that particles in large SEP events are accelerated at CME-driven shocks and *not* in solar flares (see reviews by Reames 1990a, 1992, 1993, 1994, 1995; Kahler 1992; Gosling 1993).

A recent study of the rise phase of events with protons from 470 MeV to 21 GeV (Kahler 1994a) shows that the

[1] National Research Council Senior Research Associate.
[2] Permanent address: Royal Melbourne Institute of Technology, Melbourne 3001, Australia.

events reach maximum intensity only when the shock at the leading edge of the CME reaches 5–15 solar radii. The outward speeds of these CMEs often reach 2000 km s^{-1}. These observations, as well as the charge states of Fe at 200–600 MeV amu^{-1}, lay to rest the myth that shock acceleration is, for some reason, confined to low energies. The space-time dependence of the acceleration efficiency is not the same at all energies. However, all of the particles in these events are accelerated at the shock, *not* in the flare.

For completeness, however, we should note that there are occasional large particle events directly associated with impulsive flares, generally associated with γ-ray–line events at the Sun. The energetic particles from these events have ^{3}He-rich, Fe-rich abundances (Van Hollebeke, McDonald, & Meyer 1990) and, in one case, abundances derived from broad γ-ray–line intensities produced by the energetic ion beam in the flare loops showed the same characteristic abundance enhancements (Murphy et al. 1991). Energetic particles from some magnetically well-connected events show Fe-rich abundances from the flare early in the event followed by Fe-poor abundances from the shock (Reames 1990b).

Once we realize that particles in the large gradual events are accelerated at CME-driven shocks, we can begin to use the particles to study the spatial and temporal properties of these huge evolving structures that expand out into the heliosphere. Energetic particles streaming away from the shock now become a tool that we can use to probe the strength of the shock even when it is relatively far from the observing spacecraft.

The first systematic study of the particle distribution around an evolving CME-driven shock was performed by Cane, Reames, & von Rosinvinge (1988). Using a sample of 235 proton events obtained over 18 years, they grouped the events in intervals of longitude relative to the associated flare (CME longitudes cannot be directly determined). It was then possible to understand the pattern of intensity-time profiles versus longitude in terms of the location of the strongest acceleration region near the nose of the expanding shock and the way in which the evolving magnetic field pattern allowed the observer to be connected to that region.

Statistical studies from a single spacecraft can determine the typical shape of the particle time profiles versus longitude, but unfortunately, the relative normalization of profiles at different longitudes is not clear. This normalization can be studied only by observing a single event with spatially separated spacecraft. Multispacecraft studies, on the other hand, have generally studied only the maximum intensity of protons as a function of longitude (e.g., Kallenrode, Cliver, & Wibberenz 1992). These maxima can occur several days apart, thus this practice probably dates from the days of the old diffusion models which related the peak intensity to the "solar" source strength in a simple way. Our modern paradigm affords no such luxury, since the evolving magnetic connection causes each point of observation to scan along the shock as a function of time. Only by comparing complete intensity-time profiles from several spacecraft can we develop a self-consistent model of the evolving structure.

2. THE SHOCK PARADIGM

In this section we briefly review the current paradigm for particle acceleration at CME-associated shocks and our understanding of the spatial distribution of particles as deduced from single spacecraft measurements (see reviews by Reames 1992, 1993, 1994, 1995; Kahler 1992; Gosling 1993).

In the self-consistent theory of particle acceleration by interplanetary shocks (Lee 1983; Lee & Ryan 1986), particles streaming away from the shock generate Alfvén waves that resonantly scatter subsequent particles. These particles then gain energy by repeated traversal of the shock. In the Lee theory an equilibrium is established so that the intensities of both particles and resonant waves depend only on distance from the shock. At some distance from the shock, the particle intensities decrease to the point that the intensities of self-generated waves are insufficient to maintain the scattering, thence particles stream freely away. If the number of particles leaving the shock at some energy of interest is a constant fraction of the local solar wind density, and if both the energetic particles and solar wind expand outward like R^{-2}, then the intensity of particles observed at 1 AU from approaching shock will be constant with time. These conditions are often valid for ~MeV protons and they lead to intensity-time profiles like that sketched in Figure 1*a*). For historical reasons the intensity peak near the shock where the Lee theory is obeyed is called the "energetic storm particle" (ESP) events. However, all particles in the intensity-time profile are accelerated by the shock, not just those in the ESP peak.

At higher energies the particles are less numerous and their intensities decrease further as the shock expands outward from the Sun. Thus they generate fewer waves, the particles begin to leak away, and the acceleration efficiency decreases with time. This leads to time profiles like that in Figure 1*b*. At sufficiently high energies, the resonant trap-

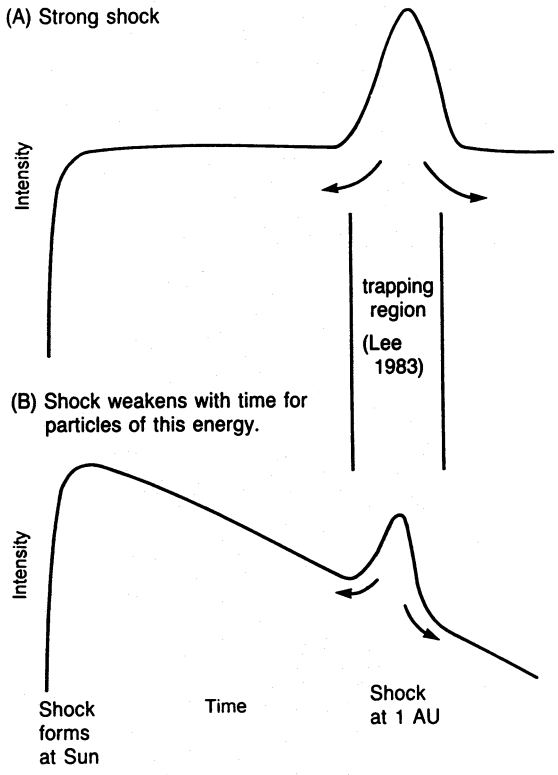

FIG. 1.—Profiles of particle intensity vs. time are shown when (*a*) strong shock acceleration continues out to the observer and (*b*) acceleration diminishes with time. *All* particles are accelerated by the shock in either case. If acceleration diminishes sufficiently the "ESP" bump may be missing.

1996ApJ...466..473R

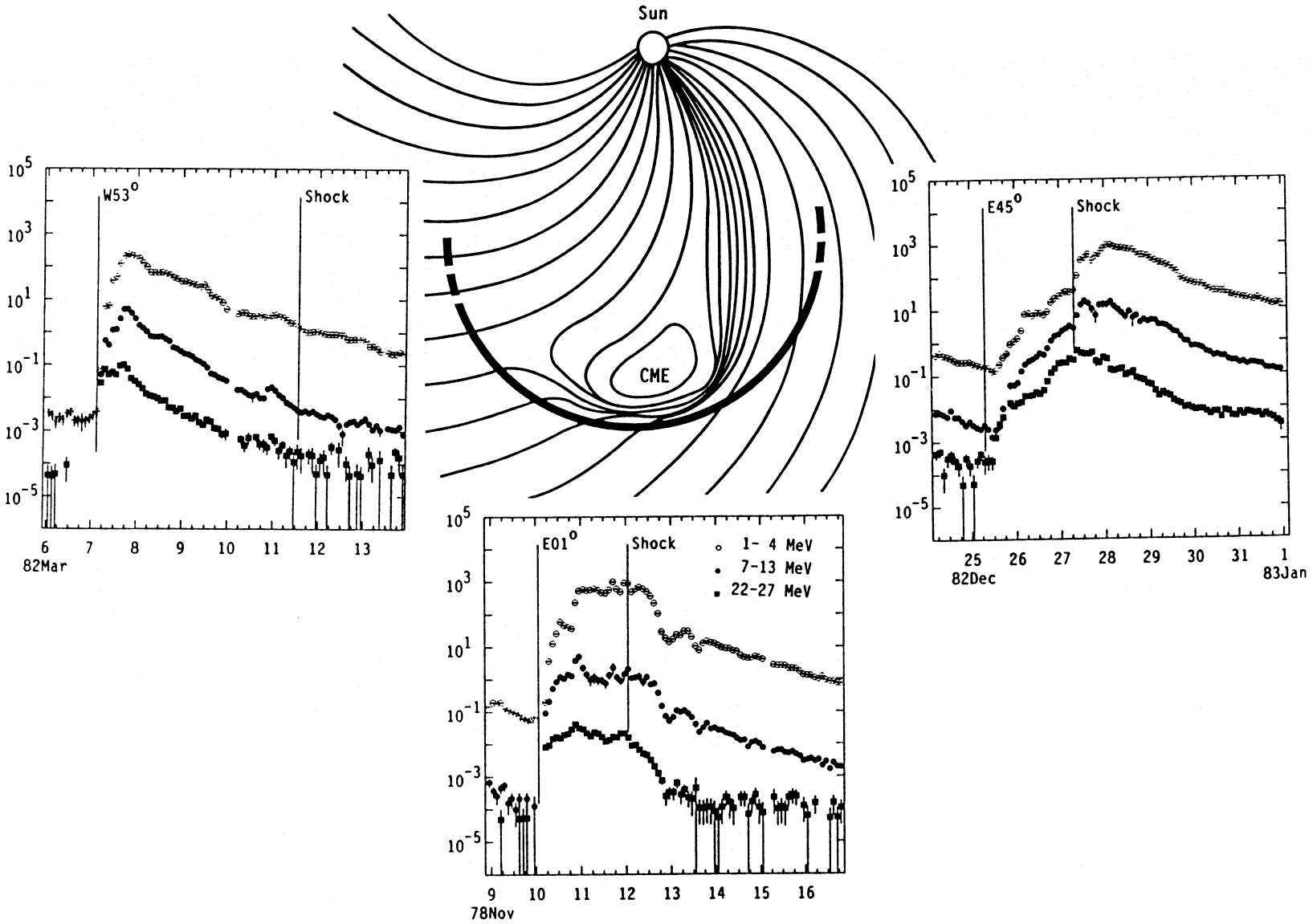

FIG. 2.—Typical intensity-time profiles for protons of three different energies are shown as seen by observers viewing a large CME-driven shock from the three different longitudes indicated. The observer seeing a western event is well connected to the nose of the shock early and sees a rapid rise and decline. Near central meridian the observer is well-connected until the shock passes; thus, he sees flat profiles. The observer viewing an eastern event is poorly connected until after the local shock passes, when he is on field lines that connect him to the powerful nose of the shock.

ping region does not survive out to 1 AU and the ESP peak is missing. At very high energies, above 1 GeV intensities may peak when the shock is at only 5–15 solar radii (Kahler 1994a).

The behavior seen in Figure 1 and described above assumes that the observer remains connected to a fixed point on the shock by a single magnetic flux tube. However, as the Sun rotates and the shock expands in heliolongitude, the observer's magnetic field of view can sweep rapidly across the surface of the shock. This results in a rapidly varying source strength during the ~2 day period of shock transit to 1 AU. Typical time profiles at 1 AU, for different observing longitudes relative to the source, are shown in Figure 2 (Cane et al. 1988; Reames 1995). An observer that views the CME from central meridian can remain fairly well connected to the central region of the shock during its transit, observing the characteristic flat profiles described above. The observer who sees the event as a western source is well-connected to the nose of the shock when it is near the Sun, but is connected to the weak eastern flank of the shock when it arrives at 1 AU. As his connection point scans to the east, he sees an increasingly weak source with time and he observes a sharply declining time profile. The third observer, on the western flank of the shock, sees the event to his east. The first particles arrive when the west flank of the shock reaches his field line in or near the corona, but his field of view scans rapidly to east toward the nose of the approaching shock, producing increasing intensities. For this observer, maximum intensities are reached only when the spacecraft has crossed the shock and encounters field lines that finally connect it to the nose of the shock which is now beyond 1 AU (Fig. 3).

Spacecraft that view an event near central meridian often encounter a region behind the shock where the intensity falls by about an order of magnitude to an intensity plateau. Bidirectional streaming of ions and electrons is often seen in this plateau region and is interpreted in terms of magnetic structures associated with ejecta from the CME itself (see Gosling et al. 1987; Marsden et al. 1987; Richardson & Reames 1993; Kahler 1994b and references therein).

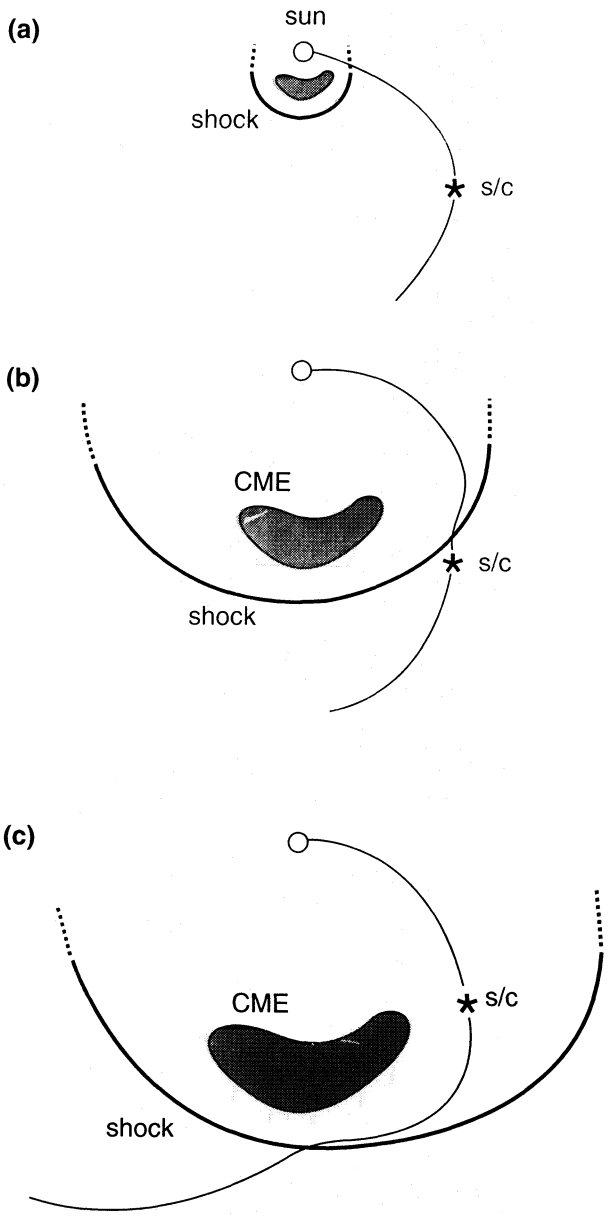

FIG. 3.—Showing schematically the spacecraft's evolving magnetic connection to the expanding shock for an eastern event. Note that the spacecraft is connected to the nose of the shock and sees an intensity maximum after the shock has traveled past it.

3. THE MULTISPACECRAFT VIEW

In this section we examine a selection of individual events where two or more spacecraft have a spatial relationship relative to the event that allows us to test the CME-shock paradigm. We present a variety of events that are not only "typical," but where others have interpreted the events according to the older diffusion paradigm. However, it has not been feasible to systematically analyze *all* SEP events because of the presence of multiple shocks and turbulent or complex interplanetary conditions prior to the event or missing data.

In the multispacecraft plots in this section, data from a particular spacecraft are always represented with the same symbol, asterisk for *Helios 1*, open circle for *Helios 2*, solid circle for *IMP 8*, and open square for *Voyager 2*. Times of interplanetary shock passage at *Helios* are taken from Volkmer & Neubauer (1985) and those from *ISEE 3* and *IMP 8* were provided by J. Gosling (private communication). Spacecraft trajectories, magnetic field, and plasma data were provided by the National Space Science Data Center. The large events that we consider are accompanied by solar flares and the multispacecraft figures contain insets showing spacecraft locations with the CME directed downward as in the sketch in Figure 2. The reader should remember that the flare is not necessarily centered on the CME and an error of ~20° or so could easily occur in this presumed CME direction.

3.1. *A "Typical" Event*

Particle intensities observed by *Helios 1*, *Helios 2*, and *IMP 8* during the event beginning 1979 March 1 at 1015 UT are shown in Figure 4. The distribution of the spacecraft, relative to the E58° event longitude, is shown in the inset of the figure. All of the spacecraft are near 1 AU. The event appears near central meridian to *Helios 1*, so it has a profile similar to that in Figure 1*a* for the 3–6 MeV protons. The rise phase is relatively slow since *Helios 1* is poorly connected when the event is near the Sun, but the characteristic flat profile at a few times 100 protons $(cm^2\ sr\ s\ MeV)^{-1}$ soon appears. The "ESP event" reaches peak intensity at

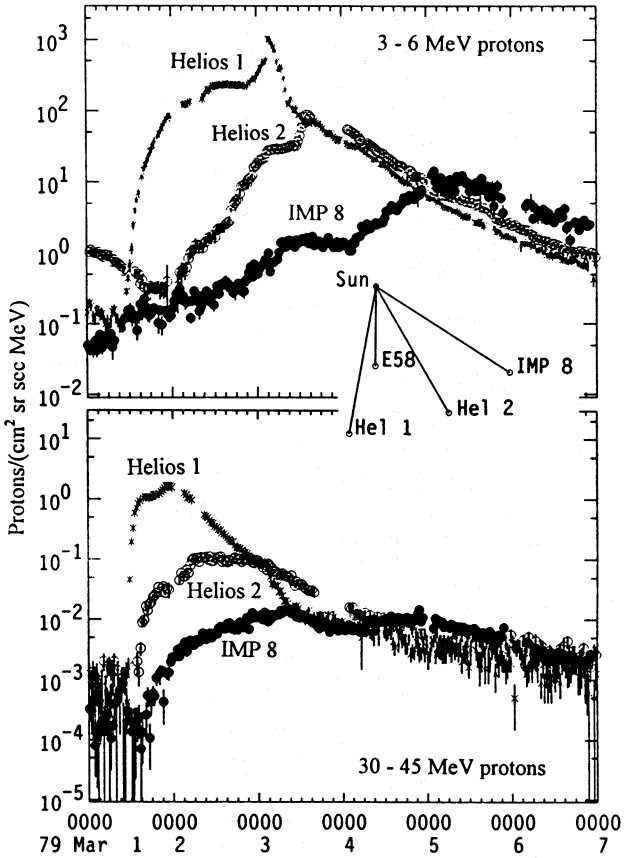

FIG. 4.—Intensity-time profiles of 3–6 MeV and 30–45 MeV protons are observed on three different spacecraft in the 1979 March 1 event. The pattern of the spacecraft relative to the nominal CME direction (downward, as in Fig. 2) is shown in the inset. The low-energy protons at *Helios 1* show the typical flat profile with an "ESP" bump that peaks at shock passage. Intensities at the other spacecraft rise slowly to meet the *Helios 1* profile as their connection to the event improves. The profiles at 30–45 MeV begin to decline when the shock is at ~0.4 AU.

shock passage at 0202 UT on March 3 (Volkmer & Neubauer 1985). *Helios 2* shows the slower rise of an eastern event as the spacecraft connection longitude scans to the east toward an increasingly strong source. About an hour after *Helios 2* crosses the shock at 0934 UT on March 3, the intensity begins a rapid rise to a peak value similar to the current intensity seen by *Helios 1*. *IMP 8* sees the event as a far eastern event (E58°). It samples the shock even farther from the nose than *Helios 2* and sees much lower intensities and a slower rise. However, after nearly 4 days of solar rotation, *IMP 8* eventually encounters the same region seen by the other two spacecraft and sees the same intensities. The intensities at all three spacecraft continue to track, within a factor of 2, until March 9, indicating an extended, highly uniform region spanning at least 60° in longitude far behind the expanding ejecta and shock.

The time profiles above 30 MeV in Figure 4 begin an earlier decline than those at 3–6 MeV, as we would expect from Figure 2*b*. The intensity of 30–45 MeV protons reaches a maximum at *Helios 1* when the shock is at ~0.4 AU. Obviously this point at which the acceleration efficiency, for a given particle energy, decreases will depend upon the shock strength. Note, however, that during the declining phase of the event, the intensities of the 30–45 MeV particles at all three spacecraft again track, within a factor of 2, just as those at lower energy.

Figure 5 shows the azimuth angle of the magnetic field and the solar wind speed along with the 3–6 MeV proton intensities in this same event. Prior to the arrival of the shock at *Helios 1*, all three spacecraft appear to be in the same magnetic sector and see similar values of the solar wind speed. Late on March 3, well after shock passage, *Helios 1* crosses into a magnetic region with opposite polarity from that seen by the other two spacecraft. For 3 days *Helios 1* remains in the magnetic sector opposite from that of *Helios 2* and *IMP 8*, yet the particle intensities on the three spacecraft track within a factor of 2! If we imagine that the CME draws out large magnetic loops with footpoints anchored at the Sun, it might be reasonable to expect that particles injected by cross-field diffusion in a turbulent region near the top of the loops might disperse uniformly into both the outward- and inward-directed legs of the magnetic loops.

Finally, note that changes in the solar wind speed before shock arrival often cause inflections in the particle intensity-time profiles. Increases in the solar wind speed straightens the magnetic field lines, causing them to connect farther east

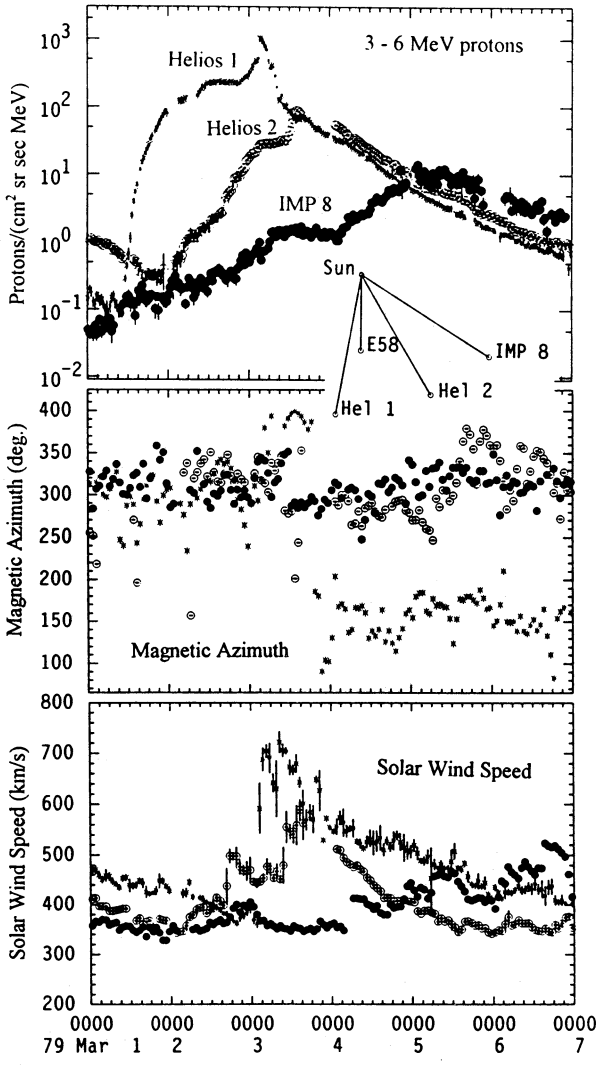

FIG. 5.—The magnetic azimuth and solar wind speed are shown together with the 3–6 MeV proton intensity for the 1979 March 1 event. The intensities at *IMP 8* and *Helios 2* become comparable with that at *Helios 1*, even though the latter spacecraft moved into the opposite magnetic sector behind the CME.

along the shock. Since the source intensity depends upon connection longitude, speed changes and intensity changes can be correlated. Such an inflection occurs in the *Helios 2* data in Figure 5, near 1700 UT on March 2, for example.

3.2. *Longitude Extent*

A much larger event with a wide longitude extent is the 1978 September 23 event, shown in Figure 6. *Helios 1* and *2* were located at 0.74 and 0.72 AU and at solar longitudes W121° and W158°, respectively. The event began at 1000 UT at W50° longitude. The shock from the event was seen at all three spacecraft on September 25 at 0229, 0133, and 0705 UT for *Helios 1*, *2*, and *IMP 8*, respectively. The event is also observed as a ground-level event (GLE) by neutron monitors, indicating the presence of multi-GeV protons. Despite some large data gaps, it is clear that the intensity-time profiles in Figure 6 show the same general characteristics as we found for those in the 1979 March 1 event in the previous section. The *Helios* spacecraft farther toward the western flank of the shock see an increasingly gradual increase in particle intensities. *IMP 8* remains "well-connected" to this huge shock event. In fact, it is even possible that the *IMP 8* instrument is saturated around the time of shock passage (the *Helios* instruments do not saturate).

Late in the 1978 September 23 event, the same particle intensities are seen on all spacecraft in both energy intervals, within a factor of approximately 2, just as we saw for the 1979 March 1 event. We will find this to be a common property of all of the events we can study in this paper. Figure 7 shows the magnetic longitude and solar wind speed for the 1979 September 23 event. It is clear that, just prior to arrival of the shock, *IMP 8* changes to a sector with the same polarity as that seen by both *Helios* spacecraft; however, there may be an intervening sector of outward polarity because of the large separation of the spacecraft. Notice the high solar wind speed at *IMP 8* on September 27–28. The particle intensities at all three spacecraft track within a factor of 2, despite the factor of 2 disparity in the solar wind speed and changes in the magnetic polarity that occur during this time.

The intensity profiles seen by a spacecraft connected to the western flank of a shock will clearly depend on the longitude extent of the CME and of the shock. For the huge event we study here, the profiles rise rapidly and remain

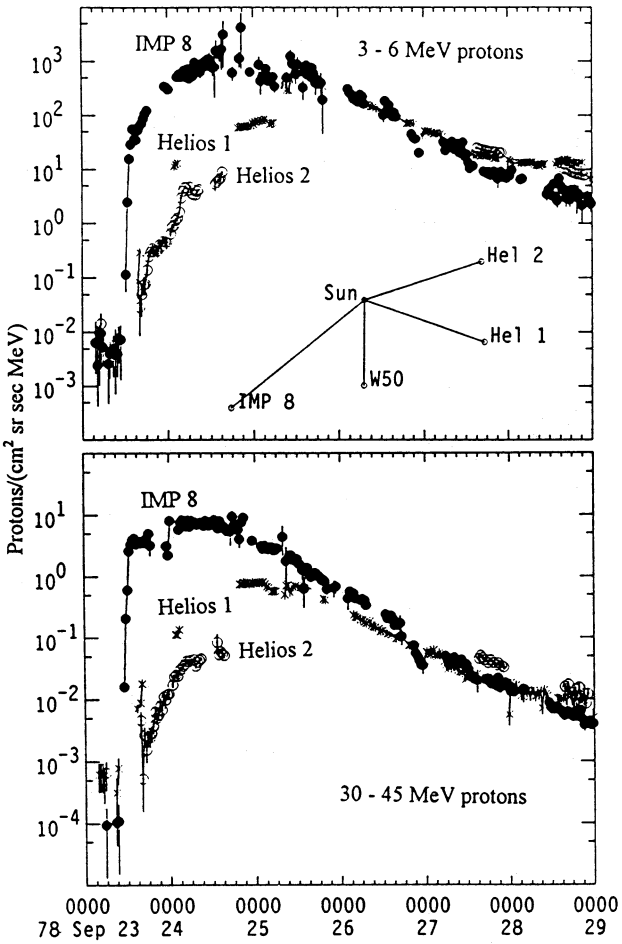

FIG. 6.—Intensity-time profiles of 3–6 MeV and 30–45 MeV protons observed on three different spacecraft are shown in the 1978 September 23 event. The inset shows the wide separation of the spacecraft in this large event. The shock itself was seen at all three spacecraft. All spacecraft show reasonably "well-connected" profiles and the intensities remain high, at high energies, until shock passage. Late in the event, the intensities at both energies are similar on all three spacecraft.

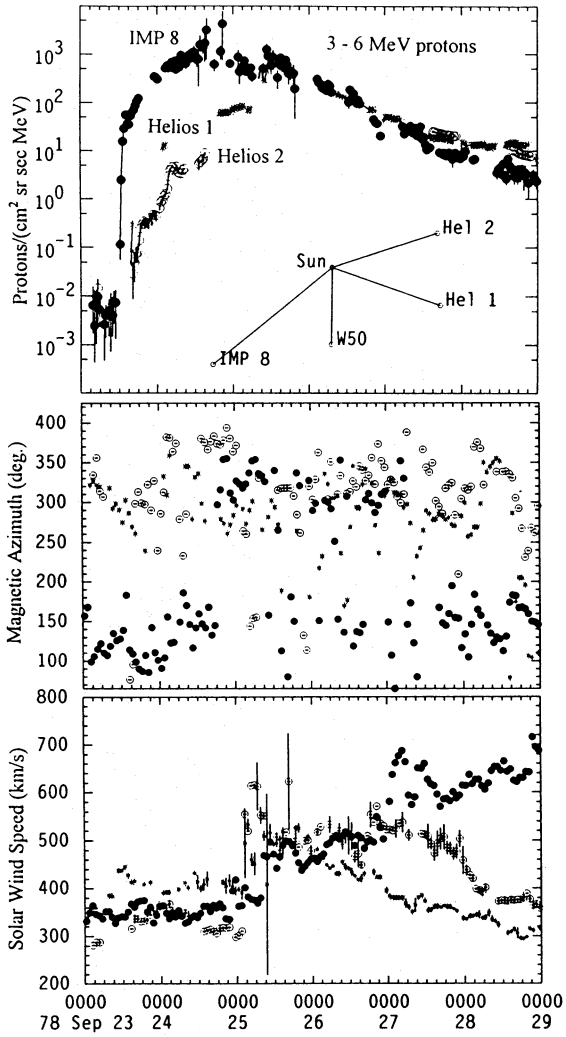

FIG. 7.—Magnetic azimuth and solar wind speed are shown together with the 3–6 MeV proton intensity for the 1978 September 23 event. Late in the event, intensities are similar at all three spacecraft despite frequent changes in the magnetic sector and large differences in the solar wind speed.

high, even for spacecraft far to the west of the event. For events with more moderate longitude extent, like the event of 1979 March 1 considered previously, spacecraft that are not very far west of the event see intensities that rise slowly and attain only modest values. We consider such observations further in the next section.

3.3. *Events with Slowly Rising Intensities*

Events with particle intensities that gradually increase over several days, as observed from a single spacecraft, have often been treated as a completely separate class of phenomenon. As such, the slow rise is presumed to represent weak and inefficient shock acceleration of inefficient transport with an extremely short scattering mean free path (Beeck & Sanderson 1989; Quenby et al. 1993; Wibberenz & Kallenrode 1995; Kallenrode 1995). In contrast, we have discussed the slowly rising profiles, like that for 3–6 MeV protons from *IMP 8* in Figures 4 or 5, as consequences of the macroscopic spatial structure of an evolving shock. Our paradigm requires that a slowly rising profile is observed from a CME source to the east; a better connected spacecraft will see a much more rapid rise, following the pattern of the events we have presented above.

An excellent example of such an event with a slowly rising profile of MeV protons is the 1978 January 1 event at 2153 UT shown in Figure 8. Viewed from a single spacecraft (*Helios 2* or *IMP 8*) in a limited energy region, as is common, many interpretations of the gradual rise might be possible. However, the profile at *Helios 1* at E39° shows the characteristic rapid rise of a well-connected spacecraft. If the gradual rise in the intensity comes from increased interplanetary scattering, must we then conclude that there is always more scattering far ahead of the shock on its western flank? This is improbable.

Magnetic field and plasma data are only shown for the *Helios* spacecraft, due to the proximity of *Helios 2* and *IMP 8*. The shock arrives at 0839 UT, 1450 UT, and 2050 UT at *Helios 1*, *2*, and *IMP 8*, respectively. Because of the moderate solar wind speed at *Helios 2* prior to the shock passage, this spacecraft is initally connected some 55° around on the western flank of the shock, relative to the flare longitude. Just behind the shock, the intensities at *Helios 2* are comparable to those seen earlier on *Helios 1*. Well behind the shock at *Helios 2*, the magnetic field undergoes the slow rotation that characterizes a magnetic cloud; this is one of the classic magnetic-cloud events reported by Zhang & Burlaga (1988) and bidirectionally streaming protons are also observed during this period (Richardson & Reames 1993).

The issue of the shock acceleration efficiency is best addressed by showing more complete energy spectra obtained at *IMP 8*, as seen in Figure 9. It would be extremely difficult to understand how a weak and inefficient shock could accelerate protons up to 100 MeV so early and so continuously during the event. We would prefer to describe the event as follows: Early in the event *IMP 8* is connected to W50° and the strong (quasiperpendicular) shock intersects the field line early, accelerating particles to high energies. As the shock propagates out, the connection to the strongest part of the shock improves so the intensities of low-energy particles increase. However, at high energies the efficiency does decrease as discussed in connection with Figure 1*b*. Therefore, *IMP 8* sees a hard spectrum with low intensities early in the event and a softer spectrum from the nose of the shock later when the shock reaches 1 AU. Actually, the time profile of 11–22 MeV protons rises fairly early and remains quite flat in Figure 9; the profile expected for constant acceleration efficiency at the source.

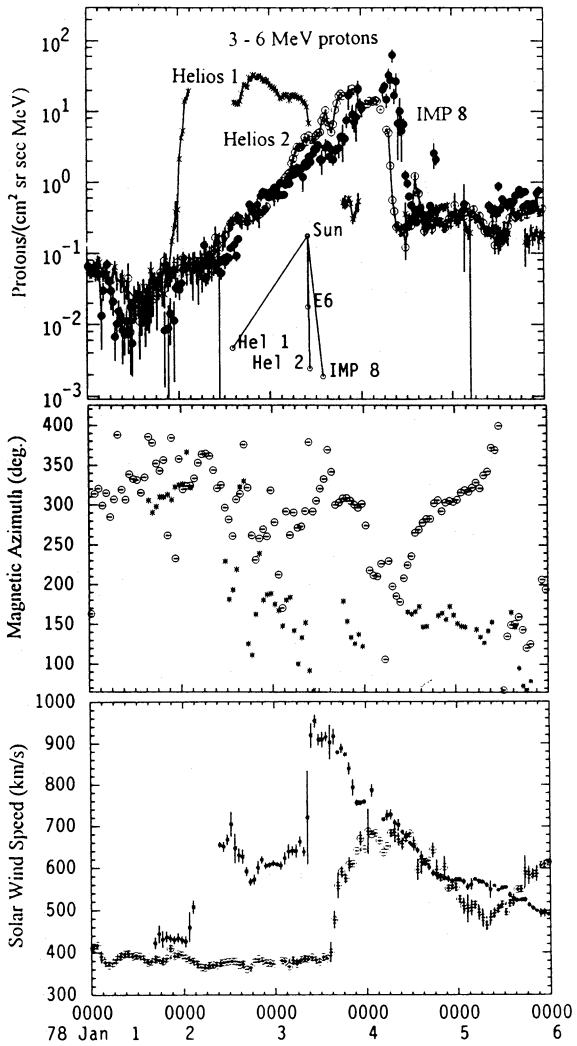

FIG. 8.—Magnetic azimuth and solar wind speed are shown together with the 3–6 MeV proton intensity for the 1978 January 1 event. The gradual rise in intensity of apparently well-connected spacecraft is produced by a CME that is relatively narrow in the ecliptic plane. The field rotation produced by this classic magnetic-cloud event can be seen at *Helios 2*. The slow rise is *not* produced by weak acceleration or inefficient transport, as can be seen in the typical profile at *Helios 1*.

In Figure 10, we show time profiles of 11–22 MeV protons in the 1980 July 17 event that occurred at 0604 UT with shock passage early on July 21. This event was observed at these energies (only on *Helios 1*) by Wibberenz & Kallenrode (1995). They describe the event as a "pure interplanetary event with slowly varying intensity," and explain the slow rise with an extremely small scattering mean free path of ~0.02 AU. From the inset in Figure 10, we see that *Helios 1* is far around on the western flank of this event (W107°) and sees the event (at E6°) as being 13° beyond its apparent east limb. *IMP 8* has a much better connection to the event and sees a moderately fast rise at this energy. Late in the event, after shock passage, both spacecraft see similar intensities, as we have come to expect. We see this as a perfectly normal event in which the spacecraft on the far western flank of the shock sees a slow rise

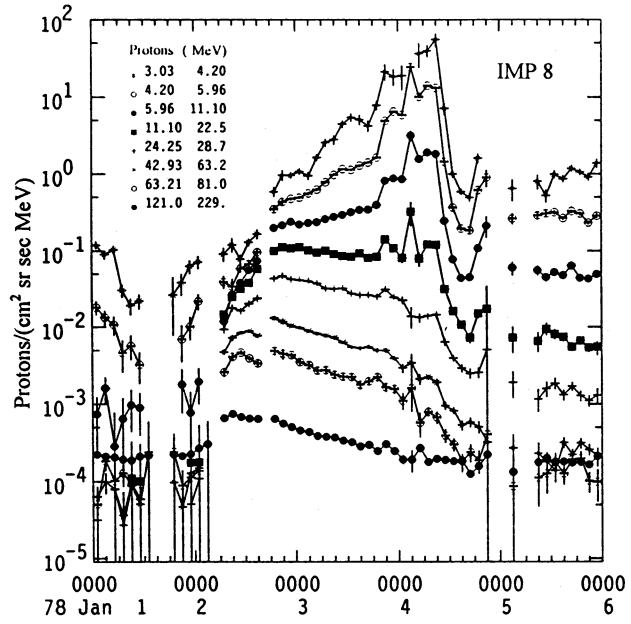

FIG. 9.—Intensity-time profiles of 3–230 MeV protons are shown in the 1978 January 1 event. The acceleration of ~100 MeV protons for ~2 days clearly shows that the slow rise at low energies does *not* come from acceleration that is too weak to accelerate 3 MeV protons early in the event. That slow rise results from an improving magnetic connection to a powerful source that is, however, slowly losing its ability to accelerate particles above ~20 MeV.

because of improving magnetic connection to stronger regions of the shock. Despite the lower intensities and poorer connection of *Helios 1* in this event, the spectra at this spacecraft (not shown) have a similar appearance to those in Figure 9. Intensities of 20–30 MeV protons rise sooner and remain flatter than those at 11–22 MeV, while the 3–6 MeV intensities rise more slowly.

We find that events with gradually rising intensity are an integral part of the spatial distribution of particles around an evolving CME-driven shock. It is simply not reasonable

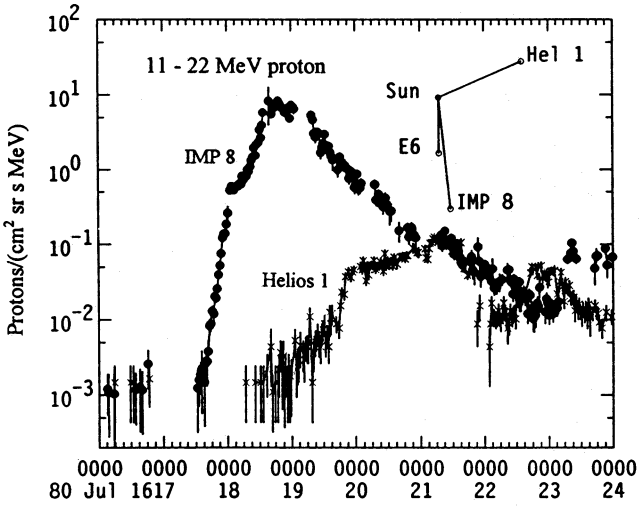

FIG. 10.—Intensity-time profiles of 11–20 MeV protons are shown for the 1980 July 17 event. The slow rise at *Helios 1* does *not* come from weak acceleration or inefficient transport as was previously proposed (see text). *Helios 1* is simply a poorly connected spacecraft viewing an event far to its east; *IMP 8* is well connected to this event and shows a correspondingly characteristic profile.

to assume that, *prior* to the onset of the shock, the interplanetary scattering mean free paths on the western flank of the shock are consistently an order of magnitude smaller than they are on the eastern flank. The preexisting scattering mean free paths resulting from fluctuations in the interplanetary magnetic fields can have no prior knowledge on which side of an emerging CME they will lie.

We would equate a "pure interplanetary event with slowly varying intensity" (Wibberenz & Kallenrode 1995) with observations of particles from a small far eastern CME-shock event. We see no need to proliferate multiple classes of proton-events based on such observations; all of the events we have discussed are interplanetary. The different profiles seem to have a purely geometric origin in a single CME-shock event where the observations are asymmetrically skewed because solar rotation affects the large-scale magnetic-field topology.

3.4. *Events with Rapidly Rising Intensities: Delayed Proton Events*

In addition to events with gradual intensity increases, there are also those with sudden increases in intensity that occur quite late in the event. Our paradigm would suggest that these observations involve a sudden improvement in the magnetic connection between the observer and a stronger acceleration region or the sudden encountering of a flux tube that already contains a particle population. Again we can use nearby spacecraft to define this preexisting condition.

Figure 11 shows a fairly small event that occurred on 1979 December 19 at 2216 UT. *Helios 1* and *2* straddle the longitude of the event. The particle intensity at *Helios 1* (at 0.63 AU) shows the normal profile of a reasonably well-connected western event. That at *Helios 2* begins an extremely slow rise more typical of a far eastern event, then, after a data gap, suddenly increased to an intensity level that is almost identical to that of *Helios 1*. If we had seen only the profile at *Helios 2*, we might have looked for a new event at the Sun; however, none exists. The nearly identical intensities strongly suggest that *Helios 2* has suddenly encountered the same population of protons that *Helios 1* has been observing for a day and a half. Notice that the very low solar wind speed (~300 km s^{-1}) would connect *Helios 2* (at 0.75 AU) to a longitude 79° west of the event, so the initial connection to this small event is poor. The solar wind speed begins to increase on December 21 and, near and behind the apparent shock position (lack of magnetic field data prevented registration of a shock at either spacecraft), *Helios 2* encounters the same magnetic environment that *Helios 1* has been seeing all along.

A more classic example of a delayed proton event is that of 1979 June 6 shown in Figure 12. In this figure a dramatic delay occurs in the onset at *IMP 8*. The event, marked by the arrow in the upper panel of Figure 12, occurred at E14° at 0514 UT on 1979 June 5, more than a day before any particle increase is seen at *IMP 8*. A key to understanding this event is again the extremely low solar wind speed on June 5, values as low as 277 km s^{-1} are seen. This would suggest that *IMP 8* is magnetically connected to W84° on the Sun, 98° west of the event. With such a long arching field line, it seems quite possible that the CME shock first contacts this field line near 1 AU, not near the Sun (a sketch of this situation is shown at the first shock position in Fig. 13, labeled for June 6). This would imply that the CME has

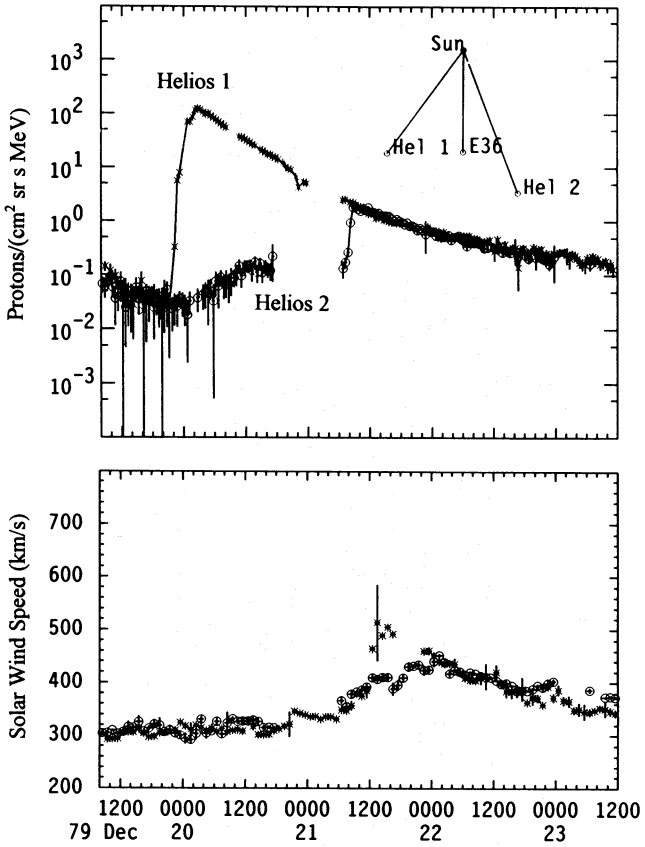

FIG. 11.—Intensity-time profiles of 10–20 MeV protons are shown the 1979 December 19 event. Because of the low solar wind speed, *Helios 2* is connected far to the west of the event. It sees few particles until it suddenly crosses to field lines behind the shock and samples the same particle population *Helios 1* has been seeing all along. This "delayed proton event" would appear as a new injection if the observations of *Helios 1* were not available.

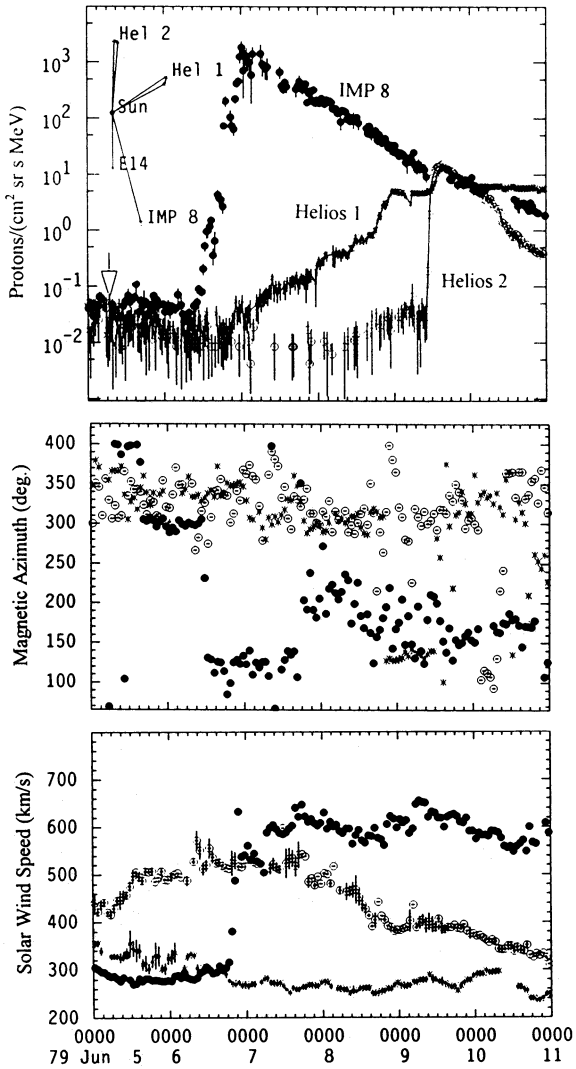

FIG. 12.—Magnetic azimuth and solar wind speed are shown together with the 3–6 MeV proton intensity for the 1979 June 6 delayed-proton event from an event at 0514 UT on June 5. *IMP 8* is in slow solar wind and sees no increase until it crosses a sector boundary prior to arrival of the shock. *Helios 1* subsequently sees a slow rise with a significant increase when it moves into the same sector as *IMP 8*. The sudden intensity increase at *Helios 2* comes from a new injection (see text).

limited longitude extent, perhaps limited by the sector boundary that passes *IMP 8* at midday on June 6. No particles are seen before this boundary crossing. Subsequently, intensities increase rapidly, peaking about 6 hr after the shock passage at 1843 UT.

After shock passage at *IMP 8*, intensities begin to increase at *Helios 1* as the field lines corotate toward it. Late on June 8 the western flank of the shock intercepts field lines connected to *Helios 1* far outside 1 AU, sending particles *sunward* toward the spacecraft. This situation is shown by the June 8 shock position in Figure 13 and the particle flow directions are seen in Figure 14. These sunward flowing particles at *Helios 1* (Fig. 14) coincide identically with the time interval that the spacecraft is in the same magnetic sector as *IMP 8* (Fig. 12).

Before this pattern can be repeated at *Helios 2*, a new event occurs far behind the limb on field lines well connected to that spacecraft. The evidence that this sudden increase is indeed a new injection includes a sudden onset of high-energy (~30 MeV) particles only at *Helios 2* (not shown), characteristic velocity dispersion in the arrival of particles at that spacecraft (not shown), and the strong outward flow of those particles shown in Figure 14.

3.5. *Radial-Azimuthal Coupling in the Evolution of Events*

A complete discussion of the radial dependence of particle transport from CME-driven shocks is far beyond the scope of this paper. Some examples of particle transport early in events have been studied using a multispacecraft observations by Mason, Reames, & Ng (1991). However, the coupling between radial and azimuthal evolution of an event becomes increasingly important as an observer moves out beyond 1 AU in the tightening spiral of the magnetic field.

As an example of this behavior, we reconsider the large event of 1978 September 23 discussed in § 3.2 with data shown in Figures 6 and 7. This time we extend the temporal and spatial scales and compare data from *Voyager 2* with that from *IMP 8* in the upper panel of Figure 15. The field lines through these two spacecraft are not widely separated, as shown in the sketch in Figure 16. However, a long gradual rise in intensity is seen as the particles accelerated at the eastern flank of the shock travel out along the field to *Voyager 2* at 4.0 AU. The classical diffusion model with an impulsive source fixed near the Sun predicts an r^{-3} decrease of the maximum intensity with heliocentric distance r. In the present situation, however, the shock-assisted particle

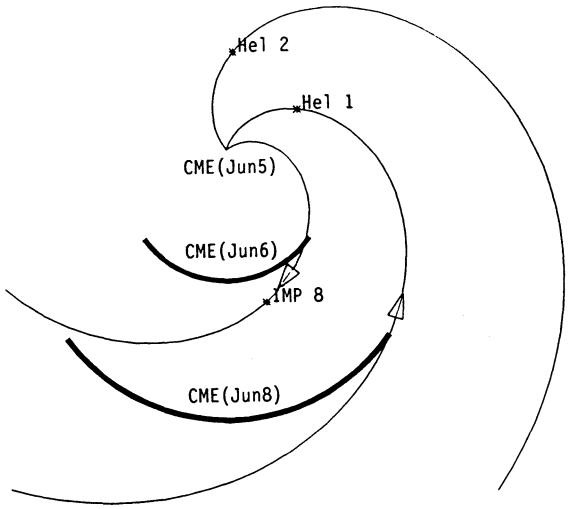

FIG. 13.—A sketch of the spacecraft, magnetic field, and shock configurations is shown for the 1979 June 6 delayed-proton event (field lines are illustrative and do *not* reflect modification by shocks). Particles are not seen until the sharp western edge of the shock strikes the field lines, sending particles outward to *IMP 8*, and later, sunward toward *Helios 1*.

source is extended in time and travels toward the spacecraft. The long injection tends to reduce the spatial falloff of the maximum intensity. On the other hand, the approaching source as well as the longitudinal gradient tend to enhance this falloff of the maximum intensity between *IMP 8* and *Voyager 2*. Apparently, the latter effects dominate. We note that for particle mean free paths greater than ~ 0.5 AU the diffusive approximation does not hold for observation at *IMP 8*.

As we noted earlier, the shock from this event is seen at all three inner spacecraft, with *Helios 2* lying 110° to the west of the flare longitude. As the CME and shock continue to propagate outward to location B in Figure 16, this *western* flank of the shock again encounters the field lines to *IMP 8* and *Voyager 2* on the right-hand edge of the figure, sending a fresh burst of particles outward toward *Voyager* and inward toward *IMP*. The azimuthal distribution of particles at *IMP 8*, shown in the lower panel of Figure 15, records the sunward flow of particles during the second broad maximum on October 4–5 (*IMP 8* data may be affected by the Earth's magnetosphere during the early part of this period; however, *ISEE 3* data confirm a sunward flow during this time). This time, with the source at ~ 3.5 AU, the intensities seen at the two spacecraft are similar.

We should note that during the long time period analyzed here, other events do occur at the Sun. Looking only at *ISEE 3* data, Richardson, Cane, & von Rosenvinge (1990) associated the second intensity increase with a small shock (local $\Delta V \approx 70$ km s^{-1}) that passed *ISEE 3* early on October 4. However, sunward particle flows are seen for nearly a day prior to the arrival of this shock and the nearly equal intensities at *IMP 8* and *Voyager* suggest a source at large distances, near *Voyager*. A source near 1 AU would produce a maximum intensity at *Voyager* more than two orders of magnitude below that at *IMP 8*.

In general, observations in the outer heliosphere are seriously complicated as a strong shock can cross and recross an observer's field line, making source identification virtually impossible. In contrast, these new injections in the outer heliosphere have a minimal effect in the inner heliosphere where they produce only small particle intensity increases.

3.6. *Time Decay Late in the Events*

Late in the events (>3 days) we have studied here, we find intensities that are nearly independent of longitude and that exhibit a quasi-exponential or quasi-power-law decay with an *e*-folding time constant of 10–20 hr. For example, in the 1978 September 23 event, the 3–6 MeV proton intensity at *IMP 8* decays quasi-exponentially with a decay time of about 14 hr. In the 1979 March 1 event, the 3–6 MeV proton intensity at *Helios 1* follows a near power-law decay with a time constant of about 12 hr on March 4, decreasing to about 24 hr on March 6.

In this section we make a crude estimate of the decay time of the particle intensity by assuming that the particles are "quasi-trapped" between the converging magnetic field near the Sun and a moving shell of strong scattering downstream of the distant traveling shock. We also assume a large particle mean free path (≥ 0.5 AU), negligible cross-field diffusion, a nearly isotropic particle distribution with negligible spatial gradient along the flux tube and a power-law energy spectrum with constant index δ. After the shock has traveled beyond the observer, if we consider only the expanding volume and adiabatic deceleration, and ignore fresh particle injection from the receding shock, we may approximate the decay of j_c, the differential particle intensity with respect to energy at a corotating point in the "quasi-trap," by

$$\frac{1}{j_c}\frac{\partial j_c}{\partial t} = -\frac{2+2\delta}{t}, \quad (r < r_o + W_r t),$$

where W_r is the postshock solar-wind velocity, and r_0 is the inner boundary of the "quasi-trap" (Appendix). With $\delta = 2.5$ (in the observed range), this gives an *e*-folding decay time of 14.3 hr (21.4 hr) at $t = 100$ hr (150 hr), roughly in agreement with the observation. We note that the small longitudinal gradient observed in the decay phase will slightly modify the decay time, and the effect of the receding particle source ignored in the present treatment should be considered in a more rigorous treatment.

The intensity-time history observed by a spacecraft as it samples progressively more eastern flux tubes must depend additionally on the longitudinal variation of the particle source strength and transport parameters associated with flux tubes that connect to different points of the traveling shock. To fit with a model the observed near-equality (to within a factor of ~ 3) of the decaying differential particle intensities at $t > 3$ days observed by spacecraft widely separated in longitude thus requires an extensive exploration of the many free parameters and functions. Fitting using conventional models with parallel diffusion is unlikely to give a consistent physical picture that explains the near-equality of the late intensities at different spacecraft in *all* our observed events. Such a fitting is not undertaken in this paper. We may need to explore alternative models, e.g., closed magnetic loops that result from magnetic-field reconnection in the CME (Gosling, Birn, & Hesse 1995). The decay of the intensity in a magnetic loop will be similar to that in an expanding quasi-trap described in the preceding paragraph. In this case we need to study how the energetic particles gain access to the magnetic loop. Finally, we note

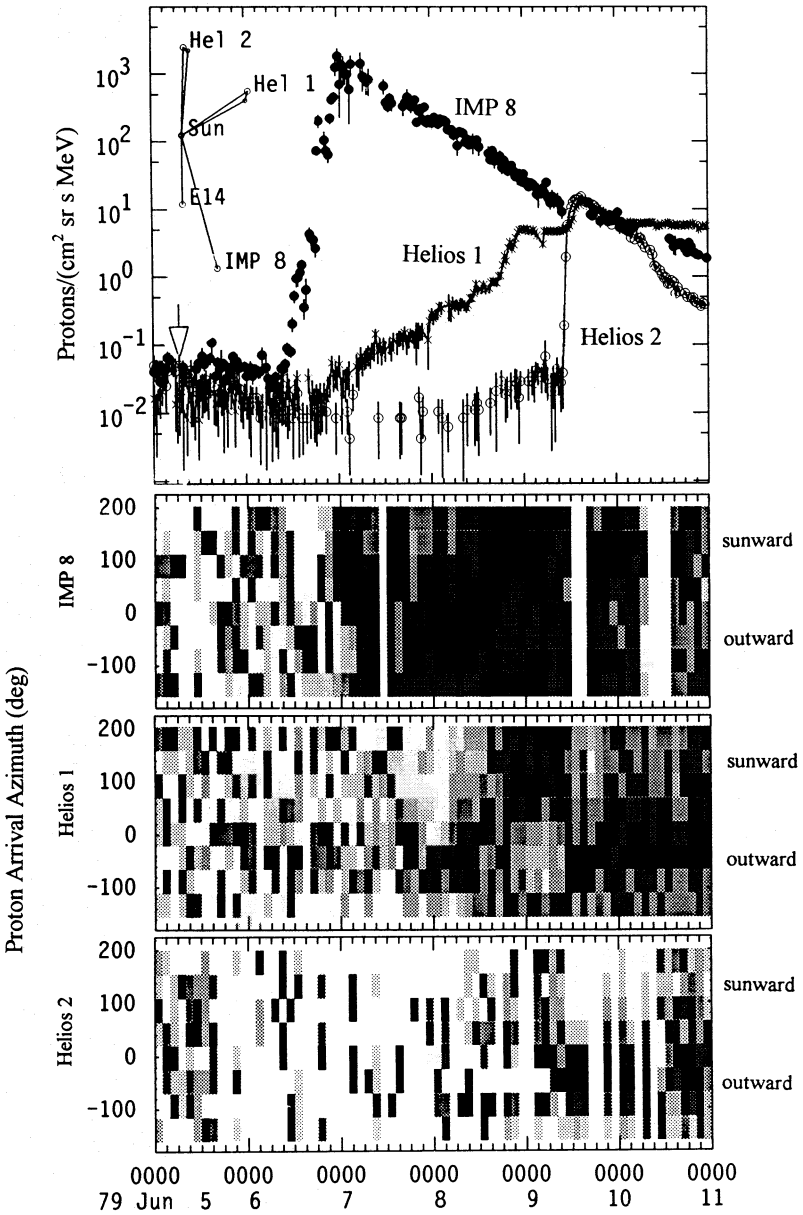

FIG. 14.—Distributions of proton arrival directions at the three spacecraft are shown during the 1979 June 6 period together with the 3–6 MeV intensity profiles. Sunward flows are seen after shock passage at *IMP 8* and early on June 9 at *Helios 1*. A new injection interupts the event at the *Helios* spacecraft at midday on June 9.

that after ~100 hr, the effect of cross-field diffusion may not be negligible.

4. CONCLUSIONS

First, it should be noted that the general features of the shock paradigm are well supported by the observations described above. The distribution of energetic particles around an evolving CME-driven shock deduced from statistical studies on a single spacecraft (Cane et al. 1988) are largely confirmed by simultaneous observations on several spatially separated spacecraft.

The dominant effect on the time profiles of 1–10 MeV protons is evolution of the intersection point between the observers magnetic field line and the shock. This point sweeps rapidly eastward across the face of the shock with time, connecting the observer to a strengthening or weakening source. The strongest acceleration occurs near the nose of the shock immediately ahead of the outbound mass ejection. Both the shock strength and the acceleration weaken around toward either flank.

Consider, for example, an observer at 1 AU who is initially connected to W55° on the Sun as a CME is launched from central meridian. The first point of intersection of the field line and shock will lie at least 55° (probably even 90°) around the shock surface to the west of the nose. Yet when this shock arrives at 1 AU, typically ~2 days later, the observer is at its nose. This simple example shows that intersection point sweeps to the east across the shock face at a rate of 27°–45° day^{-1}, far faster than one might expect from the solar rotation rate of 13° day^{-1}.

With this perspective, the longitude span of the CME becomes very important. When the CME and shock are small, rapid changes in intensity can occur, especially when the connection point sweeps across regions where the shock

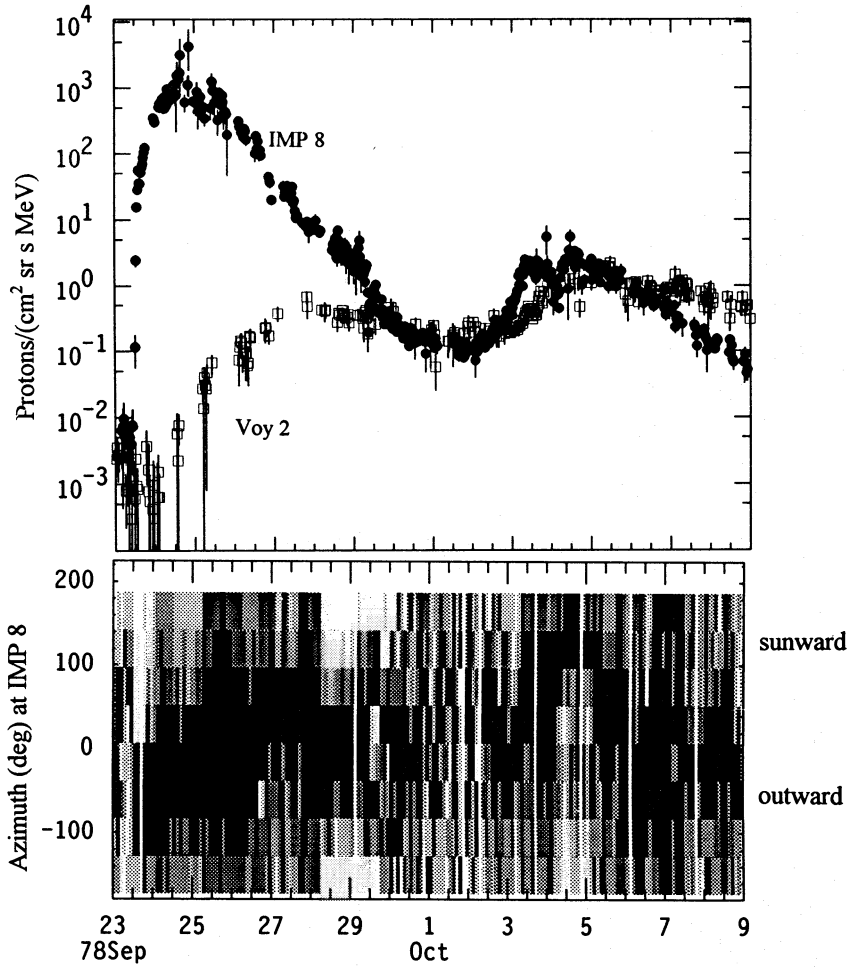

FIG. 15.—The intensity-time profiles of 3–6 MeV protons at *IMP 8* and *Voyager 2* are shown for the 1978 September 23 event both show a second increase of comparable but low intensity on October 2. The distribution of proton arrival directions at *IMP 8* shows *sunward* flows at *IMP 8* during this second maximum.

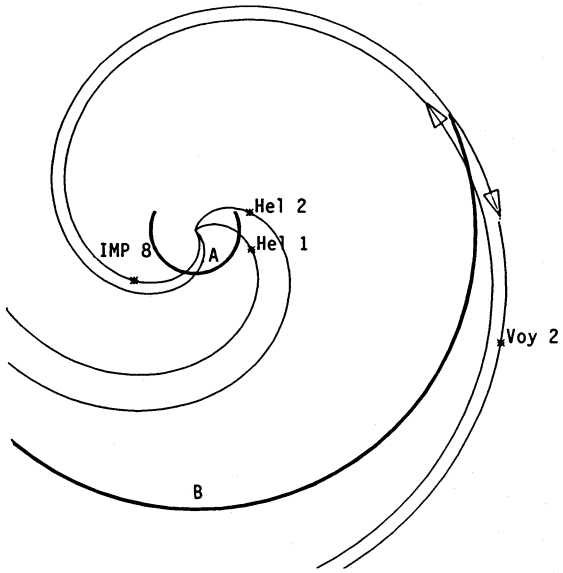

FIG. 16.—A sketch of the spacecraft, magnetic field, and shock configurations is shown for the 1978 September 23 event (field lines are illustrative and do *not* reflect modification by shocks). Early in the event particles from the eastern flank of the shock propagate outward to *IMP 8* and *Voyager 2*. On October 2 the western flank of the shock reaches the same field lines near ~4 AU, sending particles *sunward* to *IMP 8* and outward to *Voyager 2*.

strength increases or diminishes rapidly. When the CME and shock span a large interval, the longitude profiles become flat and even widely separated spacecraft appear to be reasonably "well connected." This is the case for the large 1978 September 23 event (Figs. 6, 7, 15, and 16). If we assume that this shock is symmetric about the flare longitude, then it spans an angle of at least 220°.

At energies above about 10 MeV the time profiles are also affected by decreases in the acceleration efficiency with time as the shock strength decreases and the intensity of waves resonating with these particles decreases at least as fast as r^{-2}. The radius where the shock fails to produce saturation in particle intensity, at a given energy, also depends upon longitude and upon the initial shock strength. In moderate events, ~30 MeV protons maintain near-maximum intensity until the shock reaches ~0.5 AU. Protons with ~10 GeV peak much nearer the Sun, when the shock is at ~0.05 AU (Kahler 1994a). At lower energies, however, large shocks can continue to accelerate particles far out in the heliosphere, producing sunward flowing particles as a signature of the distant source.

The lack of longitude gradient of the intensities at all energies late in an event, well behind the shock, is in striking contrast with the dramatic longitude dependence of intensities ahead of the shock. It is possible that the longitude independence late in the event results, in part, from mag-

netic loops drawn out by the CME that couple widely separated regions behind the CME. Possible patterns of three-dimensional magnetic topology in this region have been described recently by Gosling et al. (1995). This coupling may be aided by cross-field diffusion of the particles, especially in the turbulent region between the shock and the CME. We do not have a quantitative understanding of this process at present. It is likely, however, that the slow decrease in intensities late in the event results from expansion of the volume in which particles are quasi-trapped, between the converging magnetic fields near the Sun and the region of intense scattering behind the shock.

In general, we have found that the shock paradigm can explain multispacecraft observations of particle time profiles in SEP events. In fact, SEP observations provide a technique for mapping the spatial structure of an approaching shock as the observers field line sweeps across it. However, it is appropriate to note that there are still significant questions about the behavior of shocks at interplanetary boundaries, for example, where effects on the particles are sometimes large and sometimes negligible. Some of the difficulty probably lies in our inability to understand the full three-dimensional structure of the evolving CME.

The authors thank J. T. Gosling for providing lists of interplanetary shocks identified on *ISEE* and *IMP* spacecraft, and the referee for valuable comments.

APPENDIX

ESTIMATING THE DECAY TIME

The evolution of the particle distribution is governed by the transport equation in *mixed* coordinates (Ruffolo 1995)

$$\frac{\partial F}{\partial t}+\frac{\partial}{\partial z}\left[(\mu v+W_z)F\right]+\frac{\partial}{\partial \mu}\left[\frac{v}{2L}(1-\mu^2)F+\mu(1-\mu^2)\frac{dW_z}{dz}F\right]+\frac{\partial}{\partial \mu}\left(D_{\mu\mu}\frac{\partial F}{\partial \mu}\right)-\frac{\partial}{\partial p}\left\{\left[(1-\mu^2)\frac{W_z(z)}{2L(z)}+\mu^2\frac{dW_z}{dz}\right]F\right\}=0\,, \tag{1}$$

where

$$F(p,\,\mu,\,z,\,t)=\frac{4\pi p^2}{B(z)}f(p,\,\mu,\,z,\,t)\,. \tag{2}$$

We use the following notations: f denotes particle phase-space density, $\boldsymbol{B}$ mean magnetic induction, B_r radial component of $\boldsymbol{B}$, t time, z outward distance along a Parker magnetic field line, r heliocentric distance, μ pitch-angle-cosine, p particle momentum, v particle velocity, L focusing length, $D_{\mu\mu}$ diffusion coefficient in μ-space; Ω solar angular velocity, θ heliographic colatitude, ψ "garden-hose" angle between the radial direction and the outward magnetic-field direction, W_r radial constant solar-wind velocity (downstream of the shock) relative to a fixed frame, and W_z solar-wind velocity relative to a frame corotating with the Sun. The quantities z and t are referred to the fixed frame, whereas p, v, and μ are referred to the corotating frame. F may be regarded as a linear density along a narrow magnetic flux tube, and it has the same energy dependence as j_c, the differential intensity with respect to energy.

In equation (1), the second term refers to streaming and convection, the third to adiabatic focusing, the fourth to μ-diffusion, and the fifth to adiabatic deceleration. Terms associated with dW_z/dz are related to the increase of the solar-wind velocity with z as seen in the rotating frame.

A rigorous derivation of the decay time of the differential intensity j_c would require a full solution of equation (1), subject to appropriate source function, initial, and boundary conditions. This is beyond the scope of the present paper. Here, we estimate the decay time for an assumed power-law radial dependence of the particle distribution, by regarding the particles as quasi-trapped in an expanding flux tube between the high magnetic field region at $z=z_0$ near the Sun and the moving high magnetic field region downstream of the traveling shock at $z=z_b(t)$. The corresponding radii are $r=r_0$ and $r=r_b(t)$, respectively. For simplicity we ignore fresh injection from the receding shock, set $dr_b/dt=W_r$, and assume that F in the decay phase is nearly isotropic and expressible in the form: $\langle F\rangle_\mu=F_0(p,z,t)=G(z)X(t)p^{-2\delta}$.

Averaging equation (1) over μ readily yields

$$\frac{\partial}{\partial t}\langle F\rangle_\mu+\frac{\partial}{\partial z}\left[\langle(\mu v+W_z)F\rangle_\mu\right]-\frac{\partial}{\partial p}\left[\frac{pW_z}{2L}\langle(1-\mu^2)F\rangle_\mu+\frac{dW_z}{dz}\langle\mu^2F\rangle_\mu\right]=0\,. \tag{3}$$

Isotropy implies that $\langle(\mu^2)F\rangle_\mu=F_0(p,\,z,\,t)/3$, $\langle(1-\mu^2)F\rangle_\mu=2F_0(p,\,z,\,t)/3$, and $\langle(\mu v+W_z)F\rangle_\mu[p,\,z_b(t),\,t]=W_z[z_b(t)]F_0[p,\,z_b(t),\,t]$. On the other hand, the net flux must vanish at the inner boundary: $\langle(\mu v+W_z)F\rangle_\mu(p,\,z_0,\,t)=0$. For a Parker field, we have the following useful relations: $\sec\psi=W_z/W_r=B/B_r=dz/dr=(1+b^2r^2)^{1/2}$, $L=r(1+b^2r^2)^{3/2}/(2+b^2r^2)$, $W_z/L=W_r(2+b^2r^2)/[r(1+b^2r^2)]$, and $dW_z/dz=W_rb^2r/(1+b^2r^2)$, where $b=\Omega\sin\theta/W_r$, and $B_r\propto r^{-2}$.

Integrating equation (3) with respect to z from z_0 to $z_b(t)$, using the inner boundary condition, and simplifying the result, we obtain.

$$\frac{1}{F_0}\frac{dF_0}{dt}=\left\{-W_z[z_b(t)]G[z_b(t)]+\frac{2W_r(1-2\delta)}{3}\int_{z_0}^{z_b(t)}dz\,\frac{G(z)}{r}\right\}\left\{\int_{z_0}^{z_b(t)}dz\,G(z)\right\}^{-1}\,. \tag{4}$$

Now, if we assume that the differential intensity $j_c\equiv p^2f$ varies as r^n, then it follows from equation (2) that

$$G(z)=r^{n+2}(1+b^2r^2)^{-1/2}\,. \tag{5}$$

Substituting this in equation (4), noting that $r_b(t) = r_a + W_r t$, and ignoring r_a in comparison with $r_b(t)$, we obtain for $n \neq -2$ or -3,

$$-\frac{1}{F_0}\frac{dF_0}{dt} = \frac{n+3}{t}\left\{1 + \frac{4\delta - 2}{3n+6}\right\} \equiv \frac{\alpha}{t}, \tag{6}$$

implying $F_0 \propto t^{-\alpha}$. Of course, we are not at liberty to choose the radial dependence of F_0, which has to come from the solution of a complete model. Nevertheless, if scattering is weak except in the strong scattering shell near the shock, j_c would depend only weakly on r, i.e., $n \approx 0$. For $n = 0$ and $\delta = 2.5$, equation (6) gives an e-folding decay time of 14.3 hr (21.4 hr) at $t = 100$ hr (150 hr), which are in the range of observation. The approximate agreement is satisfactory, considering the nature of the crude model. The small observed longitudinal gradients late in the events suggest that they play a minor role in determining the time profile in the decay. However, the receding particle source neglected in the present crude model may be important.

REFERENCES

Beeck, J., & Sanderson, T. R. 1989, J. Geophys. Res., 94, 8769
Cane, H. V., Reames, D. V., & von Rosenvinge, T. T. 1988, J. Geophys. Res., 93, 9555
Gosling, J. T. 1993, J. Geophys. Res., 98, 18,949
Gosling, J. T., Baker, D. N., Bame, S. J., Feldman, W. C., Zwickl, R. D., & Smith, E. J. 1987, J. Geophys. Res., 92, 8519
Gosling, J. T., Birn, J., & Hesse, M. 1995, Geophys. Res. Lett., 22, 869
Hsieh, K. C., & Simpson, J. A. 1970, ApJ, 162, L191
Kahler, S. W. 1992, ARA&A, 30, 113
Kahler, S. W. 1994a, ApJ, 428, 837
———. 1994b, Third SOHO Workshop, Estes Park, CO, ed. A. Poland (ESA, SP-373), 253
Kahler, S. W., Cliver, E. W., Cane, H. V., McGuire, R. E., Reames, D. V., Sheeley, N. R., Jr., & Howard, R. A. 1987, Proc. 20th Internat. Cosmic Ray Conf. (Moscow), 3, 121
Kahler, S. W., Cliver, E. W., Cane, H. V., McGuire, R. E., Stone, R. G., & Sheeley, N. R., Jr. 1986, ApJ, 302, 504
Kahler, S. W., Sheeley, N. R., Jr., Howard, R. A., Koomen, M. J., Michels, D. J., McGuire, R. E., von Rosenvinge, T. T., & Reames, D. V. 1984, J. Geophys. Res., 89, 9683
Kallenrode, M. B. 1995, Adv. Space Res. 15, No. 8/9, 375
Kallenrode, M. B., Cliver, E. W., & Wibberenz, G. 1992, ApJ, 391, 370
Lee, M. A. 1983, J. Geophys. Res., 88, 6109
Lee M. A., & Ryan, J. M. 1986, ApJ, 303, 829
Luhn, A., Klecker, B., Hovestadt, D., & Möbius, E. 1987, ApJ, 317, 951
Luhn, A., et al. 1985, Proc. 19th Internat. Cosmic-Ray Conf. (La Jolla), 4, 241
Marsden, R. G., Sanderson, T. R., Tranquille, C., Wenzel, K.-P., & Smith, E. J. 1987, J. Geophys. Res., 92, 11,009
Mason, G. M., Reames, D. V., & Ng, C. K. 1991, Proc. 22 Internat. Cosmic-Ray Conf. (Dublin), 3, 197
Meyer, J. P. 1985, ApJS, 57, 151
Miller, J. A., & Viñas, A. F. 1993, ApJ, 412, 386
Murphy, R. J., Ramaty, R., Kozlovsky, B., & Reames, D. V. 1991, ApJ, 371, 793
Quenby, J. J., Lim, T. L., Drolias, B., Keppler, E., & Frañz, M. 1993, Proc. 23rd Internat. Cosmic-Ray Conf. (Calgary), 30, 270
Reames, D. V. 1990a, ApJS, 73, 235
———. 1990b, ApJ, 358, L63
———. 1992, in Eruptive Solar Flares, ed. Z. Svestka, B. Jackson, & M. E. Machado (New York: Springer), 180
———. 1993, Adv. Space Res. 13, No 9, 331
———. 1994, Third SOHO Workshop, Estes Park, CO, ed. A. Poland (ESA SP-373), 107
———. 1995, Rev. Geophys. Suppl., 33, 585
Reames, D. V., Dennis, B. R., Stone, R. G., & Lin, R. P. 1988, ApJ, 327, 998
Reames, D. V., von Rosenvinge, T. T., & Lin, R. P. 1985, ApJ, 292, 716
Reames, D. V., & Stone, R. G. 1986, ApJ, 308, 902
Richardson, I. G., Cane, H. V., & von Rosenvinge, T. T. 1990, Proc. 21st Internat. Cosmic-Ray Conf. (Adelaide), 5, 333
Richardson, I. G., & Reames, D. V. 1993, ApJS, 85, 411
Ruffolo, D. 1995, ApJ, 442, 861
Tylka, A. J., Boberg, P. R., Adams, J. H., Jr., Beahm, L. P., Dietrich, W. F., & Kleis, T. 1995, ApJ, 444, L109
Van Hollebeke, M. A. I., McDonald, F. B., & Meyer, J. P. 1990, ApJS, 73, 285
Volkmer, P. M., & Neubauer, F. M. 1985, Ann. Geophys., 3, 1
Wibberenz, G., & Kallenrode, M. B. 1995, Adv. Space Res. 15, No. 8/9, 393
Wild, J. P., Smerd, S. F., & Weiss, A. A. 1963, ARA&A, 1, 291
Zhang, G., & Burlaga, L. F. 1988, J. Geophys. Res., 93, 2511